Strong toroidal effects on tokamak tearing mode stability in the hybrid and conventional scenarios

To cite this article: C J Ham *et al* 2012 *Plasma Phys. Control. Fusion* **54** 025009

Plasma Phys. Control. Fusion **54** (2012) 025009 (9pp) doi:10.1088/0741-3335/54/2/025009

Strong toroidal effects on tokamak tearing mode stability in the hybrid and conventional scenarios

C J Ham, J W Connor, S C Cowley, C G Gimblett, R J Hastie, T C Hender and T J Martin

EURATOM/CCFE Fusion Association, Culham Science Centre, Abingdon, Oxon, OX14 3DB, UK

E-mail: christopher.ham@ccfe.ac.uk

Received 7 September 2011, in final form 30 November 2011
Published 19 January 2012
Online at stacks.iop.org/PPCF/54/025009

Abstract
The hybrid scenario is thought to be an important mode of operation for the ITER tokamak. Analytic and numerical calculations demonstrate that toroidal effects at finite β have a strong influence on tearing mode stability of hybrid modes. Indeed, they persist in the large aspect ratio limit, $R/a \to \infty$. A similar strong coupling effect is found between the $m = 1, n = 1$ harmonic and the $m = 2, n = 1$ harmonic if the minimum safety factor is less than unity. In both cases the tearing stability index, Δ' increases rapidly as β approaches ideal marginal stability, providing a potential explanation for the onset of linearly unstable tearing modes. The numerical calculations have used an improved version of the T7 code (Fitzpatrick *et al* 1993 *Nucl. Fusion* **33** 1533), and complete agreement is obtained with the analytic theory for this demanding test of the code.

1. Introduction

Tearing modes in tokamak plasmas are responsible for magnetic reconnection and therefore a change in the magnetic topology, with island structures being formed. These magnetic islands are undesirable because they cause the plasma pressure profile to flatten and thus degrade confinement, see review [1]. In cylindrical geometry, tearing mode stability at a particular resonant surface, is determined by a single quantity Δ'^{cyl} [2] representing the potential energy for instability residing in the current gradient. The non-dimensionalized tearing stability index at zero plasma pressure is defined as

$$\Delta'_{m/n} \equiv \left[r \frac{\psi'_{m/n}}{\psi_{m/n}} \right]_{r_s}, \tag{1}$$

where $\psi_{m/n}$ is the perturbed magnetic flux associated with the Fourier mode having poloidal mode number m and toroidal mode number n and $[f(x)]_y$ denotes $f(y+\delta) - f(y-\delta)$ for some small δ. The resonant surface $m = nq(r_s)$ (where q is the safety factor) is located at r_s.

If there is non-zero plasma pressure and toroidal or shaping effects are present, as considered in this paper, then Δ' has a more complex definition including the Mercier indices as given in appendix A, also see [3, 4]. Indeed, in a torus there is a set of resonant surfaces, due to toroidal coupling of different poloidal harmonics, and in general there is no single scalar quantity Δ' to characterize instability [5]. However, in the presence of differential toroidal rotation or significant diamagnetic effects, tearing takes place at one resonant surface at a time [6]. In such a case one can define a set of scalar quantities $\Delta'_{m/n}$ characterizing the stability of each resonant surface. A code, T7, has been developed to calculate these quantities for a toroidal plasma with elliptic and triangular shaping parameters. Although, originally its use was restricted to infinitesimal values of the shaping parameters [4], it has now been modified to accommodate realistic values of these as discussed below. However, we will focus on strong toroidal effects here and investigate shaping effects more fully in future work.

Tearing modes can form classically, when the tearing stability index, Δ', exceeds a critical value Δ'_c (Δ'_c is often large, see for example [3]), or via the triggering of a nonlinear neoclassical tearing mode (NTM) island. It is believed that NTMs are often triggered by other plasma instabilities, such as sawteeth, fishbones or edge localized modes (ELMs) that create seed islands in the plasma by forced reconnection [1]. Work on controlling NTMs has focused on removing these

triggering events, in particular sawteeth [7]. The hybrid mode of operation in a tokamak [8] does not suffer from sawteeth because it has a broad flat central current profile which produces a safety factor profile which is also flat in the plasma core region and is slightly above unity. This scenario is expected to be important for the ITER tokamak due to its ability to achieve high plasma β (the ratio of plasma pressure to magnetic pressure), a high bootstrap current and consequently long pulses and a high level of Q, the fusion power gain.

The hybrid mode has been investigated in many tokamaks and is a topic of considerable current interest. However, tearing modes still appear in hybrid scenarios and some are described as 'triggerless', or 'spontaneous' NTMs because they do not appear to have a triggering event. This has been investigated experimentally and numerically by Brennan *et al* [9–11]. These papers use the PEST3 code [12, 13] to calculate Δ' showing that it has a 'pole-like' structure as ideal marginal instability is approached, i.e. as ideal instability is approached Δ' increases rapidly. This means tearing modes could in fact be produced classically because the tearing stability index can satisfy $\Delta' > \Delta'_c$. Further it is demonstrated in DIII-D that some of the tearing modes seen do occur as the pressure approaches the ideal stability boundary [11]. On the other hand, Turco and Luce [14] have analysed over 100 DIII-D ITER baseline demonstration discharges and they found that, at constant normalized pressure, β_N, the evolution of the current profile, characterized by the internal inductance, l_i, was important for the triggering of NTMs. They do not, however, calculate Δ' for their discharges.

NSTX has also observed NTMs with no discernible trigger [15, 16]. The modes seem to have a structure which indicates coupling between the $m/n = 1/1$ and $2/1$ harmonics and so would be consistent with the mechanism discussed in this paper. Triggerless NTMs have been detected on other machines such as ASDEX [17], TFTR [18] and T-10 [19].

The paper is organized as follows. In section 2, we discuss the calculation of Δ' and how this has been implemented in various numerical codes. In section 3, we consider the case when a $q = 1$ surface is present, comparing an analytic approach with the results from T7. Section 4 treats the hybrid case in a similar manner. The results for toroidal Δ' and their implications for the presence of tearing modes in experiments for these two cases are discussed in the conclusions. The analytic equilibrium used, the definition of Δ' and the modifications to the T7 code to enable it to calculate the $\Delta'_{m/n}$ with realistic values of ellipticity and triangularity are discussed in the appendix. An example for a JET-like equilibrium is presented there.

2. The calculation of Δ'

Within a resistive MHD model tearing modes can be studied using initial value codes, but this approach is limited to cooler resistive plasma. In hotter plasma, typical of JET or ITER, the physics of the reconnecting layers (which occur at resonant surfaces where $m = nq(r)$) requires a kinetic description and there is a wide separation in scales between the mode structure in the inner reconnection layer and in the outer MHD region. For this reason it is appropriate to employ asymptotic matching techniques, where 'internal' solutions valid in the localized reconnection region that encapsulate whatever complex physics is appropriate there, are matched to the much simpler, 'external' marginal ideal MHD solutions in the regions between resonant surfaces. In toroidal, or shaped cross-section tokamak plasma these solutions have power law behaviour with respect to the distance from the resonant surface as one approaches it, the powers being characterized by the Mercier index [20]. The output from the external solution calculation is a matching matrix, whose dimension equals the number of resonant surfaces in the plasma, involving information obtained entirely from the ideal MHD solutions [5, 21]. Associated with each poloidal harmonic j, is a Δ'_j, evaluated at the jth resonant surface, r_j. This formulation can then be used in conjunction with any realistic layer models at the resonant surfaces to provide a dispersion relation for the set of tearing modes. A considerable simplification arises if there is sheared plasma flow or if diamagnetic effects are dominant at resonant layers. This means that even in a torus, a tearing mode can only reconnect at one particular surface at a time, the plasma behaviour at other resonant surfaces being the ideal MHD response, therefore all other $\Delta'_j \to \infty$ [6]. These flows are effective even if they are far less than sonic so that the ideal MHD solutions are unaffected by them. In this case all the information required from the ideal MHD solutions collapses into a single parameter, a toroidal $\Delta'_{m/n}$, generalizing the usual cylindrical MHD tearing mode stability parameter, $\Delta'^{\rm cyl}$, yet nevertheless containing toroidal coupling effects.

A number of codes have addressed the problem of calculating the Δ' appropriate to a shaped cross-section, toroidal plasma. A first attempt, PEST3 (or resistive PEST) [12, 13] used a finite element approach which is somewhat time consuming to use and is limited in the range of plasma pressure it can accommodate because of its influence on the Mercier indices. A potentially faster approach is to solve a set of radial differential equations for the toroidally coupled poloidal harmonics describing the solution and impose appropriate boundary conditions at the magnetic axis and the wall. The T3 code and an improved version TM were the first such codes constructed [22]. The TM code solved the equations for the set of harmonics corresponding to the number of resonant surfaces in the plasma, together with their upper and lower sidebands driven by toroidal coupling coefficients calculated analytically for a large aspect ratio tokamak [5]. This was followed by T7 [4] which extended T3 to describe plasma cross-sections with elliptic and triangular shaping, necessitating the following of seven coupled harmonics for each resonant surface.

Experience with this code revealed a problem also encountered somewhat later by the more ambitious DCON [23] which used a many harmonic description of realistic equilibria. The source of the problem is that as one integrates a set of basis harmonics from the magnetic axis, the higher harmonic content of these that is generated by geometric coupling rapidly dominates, since, at least near the magnetic axis, the different harmonics grow like r^m, where r is the minor radius coordinate. Consequently the original set of basis functions becomes degenerate and the method fails numerically. In [4] this limited

calculations to infinitesimal values of the shaping parameters, although this was sufficient to identify the linear response of Δ' to variations in these parameters. Glasser solved this problem with a technique in which one redefines the basis functions as one integrates outwards to prevent this degeneracy developing. This technique has now been incorporated in T7, as described in appendix A, and allows calculation with more realistic shaping parameters. However, it should be noted that T7 currently uses an approximate plasma equilibrium, i.e. accurate for large aspect ratio and weak shaping, details of which are in appendix A or see [4]. Finally, one should mention the work of Atanasiu *et al*, which has followed a similar approach, investigating the effect of a realistic, separatrix geometry in ASDEX Upgrade [24].

The T7 code has been developed as an expansion in the inverse aspect ratio and plasma shaping parameters, so one might expect their effect on Δ' to be relatively small within the validity of the code. However, there are situations when toroidicity, characterized by the inverse aspect ratio $\epsilon = a/R_0$, where a and R_0 are the minor and major radii, respectively, and shaping parameters, E for ellipticity and T for triangularity, can have a profound effect on Δ', which can deviate from the cylindrical value by a finite amount even as these tend to zero. This can occur when there is a $q = 1$ surface present in the plasma [25] and when the q-profile is just above unity but with almost zero magnetic shear in the plasma core [26], i.e. as in the hybrid mode scenario relevant to ITER. In this paper, we examine these cases, both analytically and computationally, with the T7 code and study the impact of finite β_p, the poloidal beta, on Δ'.

3. Analytic toroidal coupling of tearing modes

A first example of the strong coupling between the $(m = 1, n = 1)$ mode and higher m modes mediated by the poloidal harmonic coupling when $q_0 < 1$ (q_0 is the central value of q) is given in this section. Results are derived analytically and then reproduced numerically using the T7 code.

3.1. Coupling of the $(m = 1, n = 1)$ *and* $(m = 2, n = 1)$ *tearing modes*

The strong effect of the coupling of the $(m = 1, n = 1)$ and $(m = 2, n = 1)$ tearing modes was first documented by Bussac *et al* [27] and subsequently investigated in Connor *et al* [5]. It was shown that for a coupled tearing mode with two rational surfaces ($q = 1$ and $q = 2$) the quantities $\Delta'_{1/1}$ and $\Delta'_{2/1}$ are related by the following expression:

$$\left(\frac{1}{\Delta'_{1/1}} - \epsilon_1^2 \frac{\delta W_\mathrm{T}}{s_1^2}\right)\left(\Delta'_{2/1} - \Delta'^{\mathrm{cyl}}_{2/1}\right) + \epsilon_1^2 \left(\frac{\delta W_{12}}{s_1}\right)^2 = 0, \quad (2)$$

where $\epsilon_1^2 \delta W_\mathrm{T}$ is the potential energy of the internal kink mode [28] with

$$\delta W_\mathrm{T} = \frac{8\sigma(b-c) + 9/4(b-1)(1-c)}{16(b-c)} - \frac{6(b-1)(c+3)(\beta_p+\sigma) - 4(c+3)(b+3)(\beta_p+\sigma)^2}{16(b-c)}. \quad (3)$$

Here $\Delta'^{\mathrm{cyl}}_{2/1}$ is the cylindrical tearing mode stability index for the $m = 2$ mode. The coupling between the $m = 1$ and $m = 2$ harmonics is represented by the coupling integral

$$\delta W_{12} = \frac{1}{2}\frac{\psi_-(r_1)}{\psi_-(r_2)}\left((\beta_p+\sigma)(b+3) + \frac{3}{4}(b-1)\right), \quad (4)$$

where

$$\beta_\mathrm{p} = \frac{2}{B_\theta^2(r_1)}\int_0^{r_1}\frac{\mathrm{d}r}{r_1}\frac{\mathrm{d}p}{\mathrm{d}r}\left(\frac{r}{r_1}\right)^2, \quad (5)$$

$$\sigma = \int_0^{r_1}\frac{\mathrm{d}r}{r_1}\left(\frac{r}{r_1}\right)^3\left(\frac{1}{q^2} - 1\right), \quad (6)$$

$$s_1 = \left(\frac{r}{q}\right)\left(\frac{\mathrm{d}q}{\mathrm{d}r}\right)_{r=r_1}, \quad (7)$$

with $q(r_1) = 1$ and $\epsilon_1 = r_1/R$. Finally, the quantities

$$b = r\left.\frac{\mathrm{d}}{\mathrm{d}r}\ln\xi_-\right|_{r_{1-}}, \qquad c = r\left.\frac{\mathrm{d}}{\mathrm{d}r}\ln\xi_+\right|_{r_{1+}}, \quad (8)$$

where $\xi_\pm = [r(1/q - 1/2)]^{-1}\psi_\pm$, ψ_- being a cylindrical $m = 2$ solution for $\psi(r) = rb_r$ (b_r is the radial component of the perturbed magnetic field) vanishing at $r = 0$ and ψ_+ the one vanishing at $q = 2$. The tearing mode dispersion relation for the mode frequency, ω, follows from substituting the appropriate expressions for the layer responses, $\Delta'_{1/1} = \Delta_1(\omega)$ and $\Delta'_{2/1} = \Delta_2(\omega)$, into relation (2). In general, solving this dispersion relation will produce several possible mode frequencies and associated mode structures.

However, if we assume that there is sufficient differential rotation to only allow reconnection at one resonant layer at a time [6], then the response at the other surface can be taken to be ideal. It is therefore possible to rearrange (2) to yield

$$\Delta'_{2/1} = \Delta'^{\mathrm{cyl}}_{2/1} + \frac{\delta W_{12}^2}{\delta W_\mathrm{T}}, \quad (9)$$

if the $m = 1$ surface is taken to be ideal, i.e. $\Delta_1(\omega) \to \infty$, or if the response at the $m = 2$ surface is assumed to be ideal, i.e. $\Delta_2(\omega) \to \infty$, then

$$\Delta'_{1/1} = \frac{s_1^2}{\epsilon_1^2 \delta W_\mathrm{T}}. \quad (10)$$

The level of rotation required is much less than sonic and so δW_T will be unaffected. This means that $\Delta'_{2/1}$ can differ significantly from the purely cylindrical value, especially if the $m/n = 1/1$ mode is close to marginal ideal stability so that the second term on the right-hand side of equation (9) becomes large with a 'pole-like' structure, even if $\epsilon \to 0$.

It should be noted that the behaviour of $\Delta'_{2/1}$ very close to the pole requires more investigation. In the vicinity of the pole the layer responses at the two surfaces should be substituted into (2) and the consistent solutions found. If, for example, a semicollisional or collisionless layer theory is used, as in [6], the $\Delta'_{2/1}$ will have an imaginary part which will resolve the apparent pole-like structure. However, $\Delta'_{2/1}$ will still become very large in this region.

3.2. Coupling of the $(m = 1, n = 1)$ *with* $(m = 3, n = 1)$ *and* $(m = 4, n = 1)$ *tearing modes*

The effect of elliptic shaping is to couple the $(m = 1, n = 1)$ and $(m = 3, n = 1)$ harmonics and so this produces a similar effect to the case of the coupling of the $(m = 1, n = 1)$ and $(m = 2, n = 1)$ modes discussed in section 3.1. Thus,

$$\Delta'_{3/1} = \Delta'^{\rm cyl}_{3/1} + \frac{\delta W^2_{13}}{\delta W_{\rm T}}, \tag{11}$$

where

$$\delta W_{13} = \frac{1}{2}\frac{\psi_3(r_1)}{\psi_3(r_3)}\left[\frac{E'(r_1)}{\epsilon_1} - \frac{E(r_1)}{r_1\epsilon_1}\right][4 + b^{(3)}], \tag{12}$$

$b^{(3)}$ is the analogue of b in (8) for the $m = 3$ harmonic and ψ_3 is the flux function for the $m = 3$ harmonic vanishing at $r = 0$. The ellipticity parameter, E is related to the elongation parameter by $\kappa \approx (a + E(a))/(a - E((a))$.

Likewise, triangular shaping couples the $(m = 1, n = 1)$ and $(m = 4, n = 1)$ modes together. The couplings from ellipticity and triangularity generally have a small effect on Δ'. This is because the coupling terms δW_{13} and δW_{14} are small due to the equilibrium property that, if the shear at $q = 1, s_1$, is small, then $rE'(r) \simeq E(r)$ for elliptic shaping with a similar result holding for triangularity.

3.3. The application of the T7 code to the coupling of the $(m = 1, n = 1)$ *and* $(m = 2, n = 1)$ *tearing modes*

The strong effect of toroidicity on the tearing mode stability index given by (9) is demonstrated numerically here using the T7 code. Such a situation provides a challenging test for the code. A parabolic safety factor profile of the form $q(r) = q_0(1 + \lambda r^2/a^2)$ with $q_0 = 0.8$ and $\lambda = 3$ was used so that the safety factor at the plasma edge is $q_a = 3.2$. The pressure profile was also taken to be parabolic, of the form $p(r) = p_0(1 - r^2/a^2)$. The plasma was assumed to have a circular cross-section, i.e. $E = T = 0$. The potential energy of the internal kink mode $\delta W_{\rm T}$ as a function of $\beta_{\rm p}$ was calculated analytically for this profile and is plotted in figure 1. Note that $\delta W_{\rm T}$ passes through zero at $\beta_{\rm p} \sim 0.2$ which means that $\delta W^2_{12}/\delta W_{\rm T}$ will produce a large correction to the $\Delta'_{2/1}$ in this region.

Figure 2 shows a plot of toroidal $\Delta'_{2/1}$ calculated analytically as the pressure increases. The pole-like structure of $\Delta'_{2/1}$ as the mode approaches ideal stability with increasing plasma pressure is evident. The '×' denote T7 results which are in complete agreement with the analytic calculation. This calculation assumed an ideal layer response at the $m = 1$ layer due to differential rotation or diamagnetic effects, i.e. $\Delta'_1(\omega) \to \infty$. This assumption could be relaxed and the full dispersion relation (2) with the appropriate layer responses could be solved thus removing the apparent infinite value of $\Delta'_{2/1}$. After the pole-like structure is passed the stability index is initially large and negative and it remains negative as pressure increases further. This branch of the solution is physical if matched to an appropriate layer response, for example an ideal

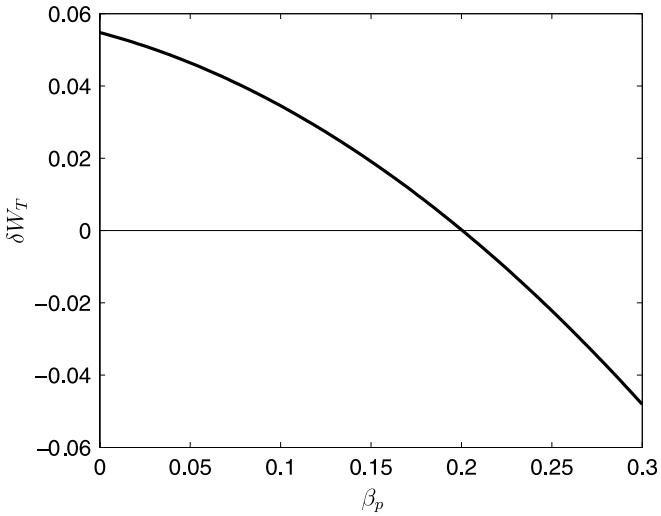

Figure 1. The $\delta W_{\rm T}$ calculated analytically as a function of $\beta_{\rm p}$ for a parabolic safety factor profile.

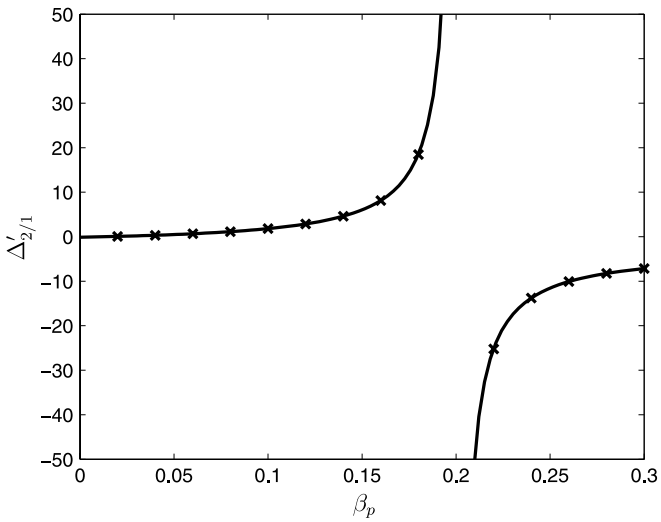

Figure 2. $\Delta'_{2/1}$ for the coupled $m/n = 1/1, 2/1$ mode with parabolic safety factor profile against increasing normalized pressure, $\beta_{\rm p}$. The continuous line is calculated analytically and '×' denotes T7 results.

response where a positive ideal growth rate would result in this region.

Figure 3 shows the T7 calculated value of $\Delta'_{2/1}$ with the parabolic profiles described above and with a fixed value of $\beta_{\rm p} = 0.15$ as the inverse aspect ratio is varied. The lower horizontal dotted line is the value of $\Delta'^{\rm cyl}_{2/1}$. The upper dotted line is the toroidal value of $\Delta'_{2/1}$ calculated analytically using (9). The solid line is calculated using the T7 code where the equations are integrated to a distance $\delta = 10^{-9}a$ from the rational surface, while for the dashed–dotted line, $\delta = 10^{-7}a$. We see that using a smaller value of δ has improved the range in ϵ over which the calculation is accurate. Figure 4 shows the calculation of $\Delta'_{1/1}$ for the same profiles assuming an ideal response at the $m = 2$ surface. The solid line shows the theoretical slope of the line implied in (10). The dotted line is calculated using the T7 code where the equations are integrated to $\delta = 10^{-9}a$ while the dashed–dotted line is for

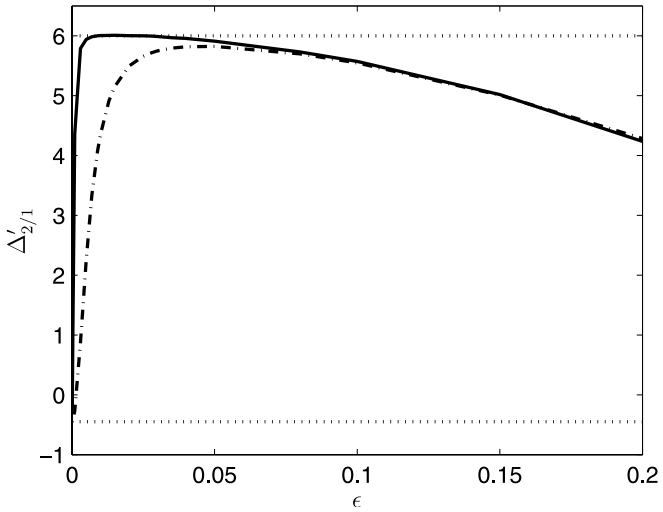

Figure 3. The $\Delta'_{2/1}$ calculated numerically using T7 against tokamak inverse aspect ratio ϵ. The lower horizontal dotted line represents the cylindrical value of $\Delta'_{2/1}$ (≈ -0.45) and the upper horizontal dotted line the analytic toroidal value from (9) (≈ 6.0). The solid line is the $\Delta'_{2/1}$ as computed by T7 with $\delta = 10^{-9}a$ and the dashed–dotted line with $\delta = 10^{-7}a$.

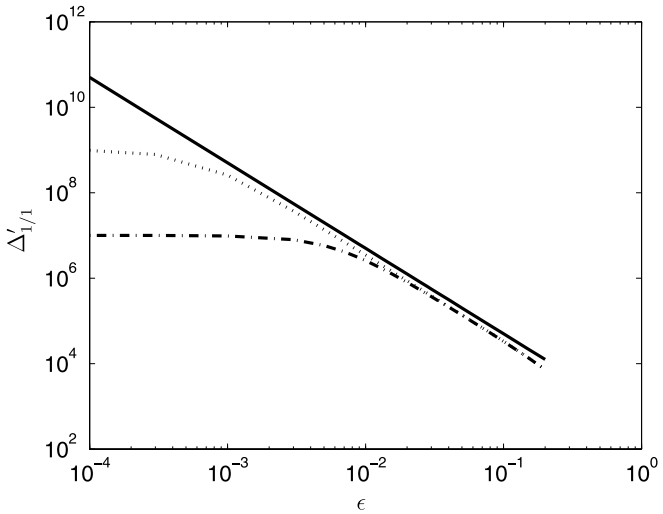

Figure 4. The dashed line plots $\Delta'_{1/1}$ as computed by T7 with $\delta = 10^{-9}a$ and the dashed–dotted line with $\delta = 10^{-7}a$ against tokamak inverse aspect ratio ϵ. The solid line shows the theoretical behaviour ($\propto 1/\epsilon^2$).

the case $\delta = 10^{-7}a$. Both these figures show that the code has difficulties as $\epsilon \to 0$. This is related to the fact that the rapid variation in the 'top hat' like eigenfunction for the $m = n = 1$ mode near $q = 1$ occurs over a width $\sim O(\epsilon)$. These calculations demonstrate that the T7 code is able to reproduce the analytic results in a certain parameter space but also highlight the need for great care with such a numerical approach.

4. Tearing stability in the hybrid scenario

The infernal mode was first mentioned by Manickam [29] and subsequently by Holties *et al* [30] and Hastie and Hender [31], in relation to low magnetic shear advanced tokamak scenarios and it is of current interest, see for example Wahlberg *et al* [32] and the investigation of the 'long-lived' mode by Chapman *et al* [26]. The hybrid scenario is also expected to be important for ITER, in part because the safety factor profile is often kept above unity, thus removing the sawtooth instability which can trigger NTMs. Given that reducing tearing mode activity is part of the motivation for this scenario, it is important to understand its tearing stability.

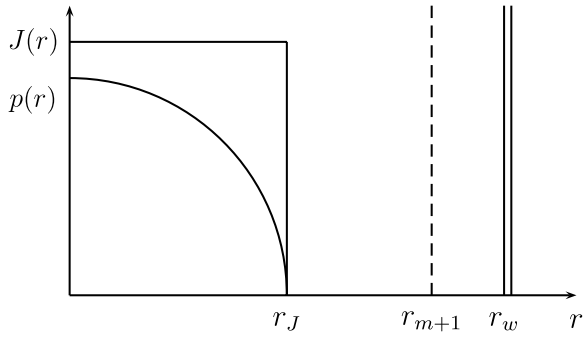

Figure 5. Current, $J(r)$, and pressure, $p(r)$, profiles used for the infernal mode. r_J characterizes the profile of $J(r)$ and $p(r)$, r_{m+1} is the resonant surface location where $m + 1 = nq$ and r_w is the wall radius.

The approach given in Connor *et al* [5] can also be applied to the infernal mode to investigate this. We consider a plasma equilibrium with a low magnetic shear region with $q \sim m/n$ (but $q > m/n$) in a region $r < r_J$. We also assume a parabolic pressure profile so that an approximate analytic expression for Δ' can be obtained. This analytic expression is then compared against numerical results from T7. This analysis shows that there can be strong toroidal coupling even if there is no $q = 1$ surface in the plasma.

4.1. Infernal mode equilibrium

A single current step

$$J(r) = J_0, \qquad r < r_J, \tag{13}$$

$$= 0, \qquad r > r_J, \tag{14}$$

and a parabolic pressure profile

$$p(r) = p_0 \left(1 - \frac{r^2}{r_p^2}\right), \tag{15}$$

where we set $r_p = r_J$ for simplicity, are assumed, in order to make this model of the infernal mode analytically tractable. These current and pressure profiles are shown in figure 5. Conducting plasma is assumed to continue beyond r_J to r_w, the wall location. The safety factor profile for this equilibrium is

$$q(r) = q_0, \qquad r < r_J, \tag{16}$$

$$= q_0 \frac{r^2}{r_J^2}, \qquad r > r_J, \tag{17}$$

where q_0, the central value of q, is a function of J_0. The safety factor profile is plotted in figure 6. It will also be assumed that the mth harmonic is almost resonant ($m \approx nq(r)$) in the plasma where $J = J_0$, but is never actually resonant because we suppose q_0 is just above m/n. However, the $(m + 1)$th harmonic is resonant at $r_{m+1} > r_J$.

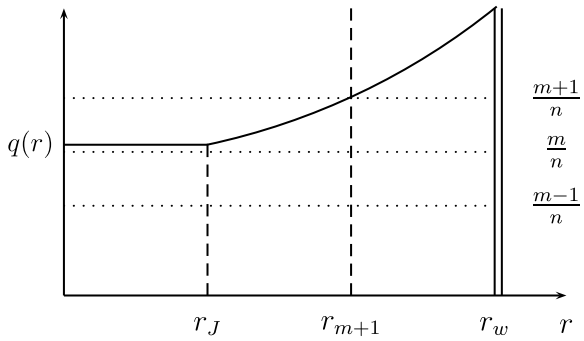

Figure 6. Safety factor profile for the infernal mode also showing the position of the resonant surface r_{m+1}.

4.2. Equation and boundary conditions for the coupled harmonics

The problem is again solved in terms of $\psi(r)$. The main poloidal harmonic and the two adjacent poloidal harmonics are described by a system of coupled differential equations, which are (A17)–(A20) in appendix A in [5]. Assuming that the mth harmonic is nearly resonant in the core region means that $1/(m - nq(r)) \gg 1$ within this region. This factor appears in some of the terms of (A17)–(A20) and so it acts as a 'magnifying factor'. All terms from [5] (A17)–(A20) which do not have $m - nq(r)$ in the denominator can thus be consistently neglected.

The mode calculation is split into several regions. For $r < r_J$ the three harmonics are coupled. The coupled differential equations for ψ_{m-1}, ψ_m and ψ_{m+1}, respectively, are

$$\begin{aligned}
&\frac{\mathrm{d}}{\mathrm{d}r}\left(r\frac{\mathrm{d}\psi_{m-1}}{\mathrm{d}r}\right) - \frac{(m-1)^2}{r}\psi_{m-1} = \frac{\hat{\beta}}{r_\mathrm{p}}\left(-r\frac{\mathrm{d}\psi_m}{\mathrm{d}r} + m\psi_m\right),\\
&\frac{\mathrm{d}}{\mathrm{d}r}\left(r\frac{\mathrm{d}\psi_m}{\mathrm{d}r}\right) - \frac{m^2}{r}\psi_m - 2\frac{\hat{\beta}^2 r}{r_\mathrm{p}^2}\psi_m\\
&\quad = \frac{\hat{\beta}}{r_\mathrm{p}}\left(r\frac{\mathrm{d}\psi_{m-1}}{\mathrm{d}r} - (m-1)\psi_{m-1}\right.\\
&\qquad \left. + r\frac{\mathrm{d}\psi_{m+1}}{\mathrm{d}r} + (m+1)\psi_{m+1}\right),\\
&\frac{\mathrm{d}}{\mathrm{d}r}\left(r\frac{\mathrm{d}\psi_{m+1}}{\mathrm{d}r}\right) - \frac{(m+1)^2}{r}\psi_{m+1} = \frac{\hat{\beta}}{r_\mathrm{p}}\left(-r\frac{\mathrm{d}\psi_m}{\mathrm{d}r} + m\psi_m\right),
\end{aligned} \tag{18}$$

where

$$\hat{\beta} = \frac{R_0}{r_\mathrm{p}}\frac{2p_0 q_0^2}{B_0^2}\frac{m}{m - nq_0} \tag{19}$$

is the coupling parameter due to finite plasma pressure.

The equation to be solved outside the current step, i.e for $r > r_J$, is

$$\frac{\mathrm{d}}{\mathrm{d}r}\left(r^{1-2l}\frac{\mathrm{d}}{\mathrm{d}r}(r^l\psi_l)\right) = 0, \tag{20}$$

where $l = m-1, m, m+1$. The solutions of this equation are of the form $\psi_l = A_l r^l + B_l r^{-l}$, with A_l and B_l to be determined. There is no coupling between the solutions in this region since the pressure goes to zero.

The solutions are matched across the current step at r_J and resonance at r_{m+1} through jump conditions. The current step jump condition is calculated by integrating the ideal MHD equations from outside the step to inside the step

$$\left[r\frac{\mathrm{d}\psi_l}{\mathrm{d}r}\right]_{r_J} - \frac{l^2}{r}[\psi_l]_{r_J} = \frac{l\mu_0 r_J \psi_l}{B_\theta(l - nq_0)}[J_0]_{r_J}. \tag{21}$$

This simplifies to give the jump condition

$$\left[\frac{r\psi_l'}{\psi_l}\right]_{r_J} = \frac{-2l}{l - nq_0}. \tag{22}$$

The boundary condition at the wall is

$$\psi_l(r_w) = 0. \tag{23}$$

Finally there is a jump condition at the resonant surface for the $(m+1)$th harmonic, given by

$$\Delta'_{m+1} \equiv \left[\frac{r\psi'_{m+1}}{\psi_{m+1}}\right]_{r_{m+1}}. \tag{24}$$

4.3. Tearing mode stability index

The tearing mode stability index resulting from solving equations (18) with the boundary and jump conditions above is

$$\begin{aligned}
&\frac{\Delta'_{m+1}}{2(m+1)}\\
&= \frac{-\hat{\beta}^2(1-2Y) + 4(m+1)(m+2)Y}{(\hat{\beta}^2(1-2X) - 4(m+1)(m+2)X)(1 - (r_{m+1}/r_w)^{2m+2})},
\end{aligned} \tag{25}$$

where

$$X = \left(\frac{m}{m+1}\right)^{m+1}, \qquad Y = X\left(\frac{r_{m+1}}{r_w}\right)^{2m+2}. \tag{26}$$

This result has been reported previously [33, 34].

Figure 7 shows the analytic tearing stability index with increasing normalized pressure (solid line) calculated for $m = n = 1$, $q_0 = 1.01$, $r_J = 0.65$ and $E = T = 0$. The ideal stability limit, when $\Delta' \to \infty$, can clearly be seen at $\hat{\beta} \approx 3.5$. Numerical results calculated using T7 are shown with '×'. These are a close match to the analytical curve even though several adjustments have been made to the analytical profiles to make them computable. Thus the profile for $q(r)$ is generated from a current profile that is slightly smoothed to avoid a sharp discontinuity in $J(r)$ at $r = r_J$ which leads to a discontinuity in the second derivative of $q(r)$; this would cause difficulties for T7.

The ideal and tearing stability limits of the infernal mode can be investigated using the dispersion relation (25). Thus, the plasma is ideally unstable when

$$\hat{\beta} > \sqrt{\frac{4(m+1)(m+2)X}{1-2X}}. \tag{27}$$

Assuming that the marginal point of stability of the infernal tearing mode is given by $\Delta' = 0$, if cylindrical single fluid MHD is considered, this corresponds to

$$\hat{\beta} > \hat{\beta}_c = \sqrt{\frac{4(m+1)(m+2)Y}{(1-2Y)}}. \tag{28}$$

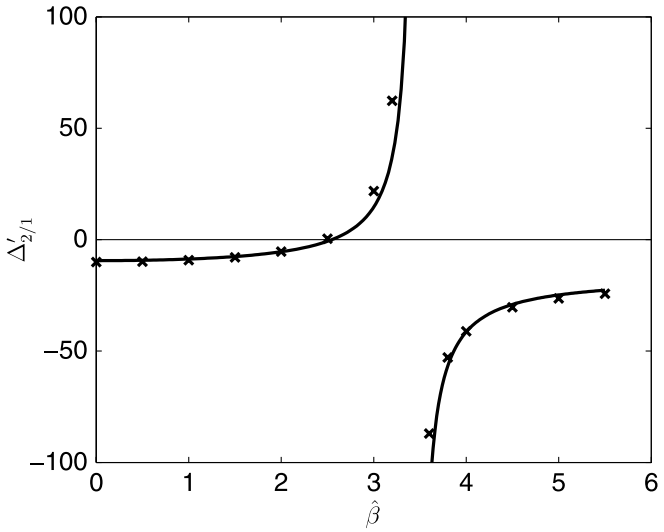

Figure 7. $\Delta'_{2/1}$ for the infernal mode against increasing normalized pressure, $\hat{\beta}$. The continuous line denotes the analytic approximation (25) and '×' denotes the result from T7.

It should be noted that taking $\Delta' = 0$ as the tearing mode stability criterion is a major simplification. It assumes an elementary layer theory with no pressure gradient or diamagnetic effects, for example. The true stability criterion would be $\Delta' > \Delta'_c$ where $\Delta'_c \gg 1$; various more realistic plasma models lead to a range of expressions for Δ'_c, see Drake *et al* [35] and Cowley *et al* [36].

5. Discussion and conclusions

There is a strong coupling effect between the $(m = 1, n = 1)$ and $(m = 2, n = 1)$ harmonics when there is a $q = 1$ surface present which means that a toroidal calculation does not reproduce the cylindrical results even as the aspect ratio tends to zero. This was investigated analytically and numerically using the T7 code. The numerical results closely matched the analytical results, even down to very small inverse aspect ratio, demonstrating that T7 is accurate in this case for realistic inverse aspect ratios. An analytic model of the infernal mode was produced and this result was also compared with numerical T7 results which were again in agreement. Thus the T7 code accurately reproduces analytic results for two different pressure and safety factor profiles of interest for ITER, cases which provide a demanding test of the numerical code. In both the cases investigated here we see that the cylindrical limit is not recovered in the large aspect ratio limit.

Near an ideal stability limit, $\beta = \beta_c$, the toroidal Δ' has a 'pole-like' structure $\Delta' \propto 1/(\beta - \beta_c)$, as demonstrated for the two current profiles investigated here. This means that as the ideal instability limit is approached Δ' increases rapidly and moreover that Δ' will exceed some critical value Δ'_c, even if $\Delta'_c \gg 1$, such that a classical tearing mode begins to grow. This is relevant to experimental observations where triggerless NTMs appear when the plasma pressure is near the ideal pressure instability proxy $4l_i$. This approach to ideal instability occurs at $\beta \sim \epsilon^2$ for the conventional scenario and $\beta \sim \epsilon(m - nq_0)/m \ll \epsilon$ for the hybrid scenario, whereas one normally expects the ideal threshold to occur for $\beta \sim \epsilon$. The results here provide analytic insights into the mechanism proposed by Brennan *et al* [9–11].

NTMs reduce tokamak confinement and so it would be advantageous to suppress them. Therefore, much attention has focused on removing NTM triggers, such as sawteeth, and the high performance hybrid mode, which does not suffer from sawteeth, has been considered a useful potential mode of operation for future machines such as ITER. However, the work here shows that even without sawteeth or other mode triggers, tearing modes can form if the plasma is close to ideal instability, and would persist as NTMs even if Δ' were subsequently reduced to a value less than Δ'_c.

The T7 code has been improved so that it can deal with realistic values of ellipticity and triangularity and will be used in a later paper to explore more generally the influence of plasma shaping on tearing mode stability. The code currently uses a large aspect ratio analytic approximation to the plasma equilibrium. However, the trends of stability with shaping and other properties should be realistic.

Acknowledgments

The authors thank A H Glasser for very useful discussions during a visit to Culham and in particular for the suggestion of using 'fixups' discussed in appendix A.3. The authors also acknowledge T O'Gorman, Y Q Liu, F Militello and I T Chapman for helpful discussions and suggestions.

This work was funded by the RCUK Energy Programme under grant EP/I501045 and by the European Communities under the contract of Association between EURATOM and CCFE. The views and opinions expressed herein do not necessarily reflect those of the European Commission.

Appendix A. T7 code and augmentations

A.1. Analytic equilibrium

The T7 code currently uses a large aspect ratio analytic equilibrium rather than the output plasma equilibrium from a Grad–Shafranov solver. The full details of this plasma equilibrium are presented in [4]; however, we give brief details here. A plasma equilibrium is constructed with coordinates (r, θ, ϕ) which are related to cylindrical coordinates (R, ϕ, Z), where Z is in the direction of the symmetry axis, by

$$\begin{aligned} R &= R_0 - r\cos\omega - \Delta_S(r) + E(r)\cos\omega \\ &\quad + T(r)\cos 2\omega + P(r)\cos\omega, \\ Z &= r\sin\omega + E(r)\sin\omega + T(r)\sin 2\omega - P(r)\sin\omega, \end{aligned} \tag{A.1}$$

where ω is the poloidal angle around the magnetic axis, Δ_S is the Shafranov shift, E is the flux surface ellipticity and T is the flux surface triangularity. The quantity

$$P(r) = \frac{1}{8}\frac{r^3}{R_0^2} + \frac{1}{2}\frac{r}{R_0}\Delta_S - \frac{1}{2}\frac{E^2}{r} - \frac{T^2}{r} + O(\epsilon^3 a) \tag{A.2}$$

is chosen so that the Jacobian of the transformation $(r, \theta, \phi) \to (R, \phi, Z)$ is given by

$$(\nabla r \wedge \nabla\theta \cdot \nabla\phi)^{-1} = \frac{rR^2}{R_0}. \tag{A.3}$$

The equilibrium coordinate θ is related to ω by

$$\theta = 2\pi \int_0^{\omega} \frac{J\mathrm{d}\omega}{R} \Big/ \oint \frac{J\mathrm{d}\omega}{R}, \tag{A.4}$$

where $J = (\partial R/\partial\omega\partial Z/\partial r - \partial R/\partial r\partial Z/\partial\omega$ is the Jacobian for $(R, Z \to r, \omega)$. The field lines appear straight in the (r, θ, ϕ) system, i.e. $B.\nabla \propto (\frac{\partial}{\partial\theta} - q(r)\frac{\partial}{\partial\phi})$.

The ellipticity parameter is related to the elongation parameter by $\kappa \approx (a+E(a))/(a-E((a))$ and the triangularity parameters are related by $\delta \approx 4T(a)(a^2 - 3T(a)^2)/a^3$.

A.2. Definition of Δ'

In the presence of pressure and toroidal effects the Δ' needs to be more carefully defined than the expression given in (1). Full details of this are given in [4]. The resonant perturbed-flux harmonics near to their rational surface behave as

$$\psi_m \approx A_\mathrm{L}|x|^{\nu_\mathrm{L}}[1 + \lambda_L x + \cdots] + A_\mathrm{S}\,\mathrm{sgn}(x)|x|^{\nu_\mathrm{S}}[1 + \cdots] + A_C x[1 + \cdots] \tag{A.5}$$

where $x = (r - r_m)/a$. The coefficients of the 'large' and 'small' solutions in the Newcomb sense [37] are A_L and A_S, respectively. The coefficients of the 'continuous' solution are A_C. The indices, ν_L and ν_S, are given by

$$\begin{aligned} \nu_\mathrm{L} &= \tfrac{1}{2} - (-D_\mathrm{M})^{1/2}, \\ \nu_\mathrm{S} &= \tfrac{1}{2} + (-D_\mathrm{M})^{1/2}, \end{aligned} \tag{A.6}$$

where D_M is given in [5], $D_\mathrm{M} > 0$ corresponding to the Mercier instability criterion.

T7 is restricted to stability calculations of the tearing parity modes where the coefficient of the large solution is continuous across the rational surface. However, the coefficient of the small solution is not continuous and this provides the definition of Δ' as

$$\Delta' \equiv \left(\frac{A_{\mathrm{S}+} - A_{\mathrm{S}-}}{A_\mathrm{L}}\right), \tag{A.7}$$

where $A_{\mathrm{S}+}$ is the amplitude of the small solution as the rational surface is approached from the right and $A_{\mathrm{S}-}$ from the left. A_L is the amplitude of the large solution at the rational surface.

A.3. Basis set re-orthogonalization

The T7 code numerically integrates a system of 14 coupled first order differential equations, as detailed in [4]. For each resonant surface in the plasma the code launches seven basis functions each with a different dominant poloidal harmonic from the integration starting point and a further one from the resonant surface. These basis functions are then combined to give a solution which satisfies the boundary conditions.

Integration of the equations is started at a small distance, r_ϵ, from the coordinate singularity at the magnetic axis. It was noticed that the code failed to run if r_ϵ was too small because the basis functions rapidly became colinear as the mth harmonic component grew like r^m and the higher m contributions dominated each basis function. It is desirable to be able to start the code from small values of r_ϵ so that numerical convergence of the code can be investigated. This situation does not arise with T3 where only toroidal coupling is present.

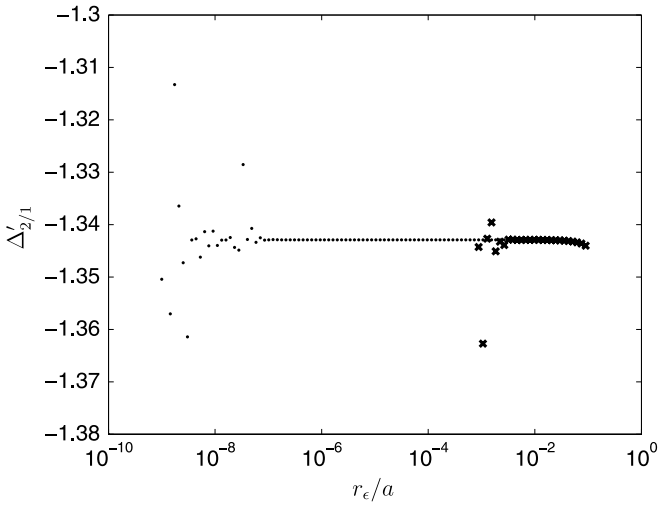

Figure A1. $\Delta'_{2/1}$ for the JET-like equilibrium described in the text as the starting point of the integration, r_ϵ, changes. Two re-orthogonalization points have been used in calculating the '·' points, one half way between r_ϵ and 0.1 and one at 0.1. No re-orthogonalizations were used calculating the '×' points.

A scheme similar to Glasser's 'fixups' [38] is employed to re-orthogonalize the basis set. These are implemented in T7 at user defined locations between the magnetic axis and the first resonant surface. These re-orthogonalizations are not used (and indeed are not necessary) beyond the first resonant surface so that the jump conditions remain unchanged. At each re-orthogonalization location the matrix of basis functions is forced to become upper triangular, via a process similar to Gaussian elimination, such that only one basis function has a non-zero amount of the seventh harmonic, two basis functions have non-zero sixth harmonic content and so on. The basis functions are then renormalized to their largest component. Figure A1 shows the difference between no re-orthogonalizations '×' and the use of two re-orthogonalizations '·'. A significant improvement can clearly be seen.

A.4. JET-like Δ' *calculation*

An example calculation of $\Delta'_{2/1}$ with T7 has been carried out here using typical values of elongation, $\kappa = 1.8$, and triangularity, $\delta = 0.25$, for a JET-like plasma. A parabolic safety factor profile has been used with $q_0 = 1.2$ and $q_a = 2.8$. A parabolic pressure profile has also been used with a small value of core pressure, $\beta_0 = 0.01\%$. The inverse aspect ratio used was $\epsilon = 0.324$, again a JET-like value.

Figure A1 shows how $\Delta'_{2/1}$ changes as the integration starting point r_ϵ is moved closer to the magnetic axis. The code is well converged until $r_\epsilon \approx 10^{-7}a$ when two re-orthogonalizations are used, '·'. An improvement of several orders of magnitude can be seen from the case when re-orthogonalization are not used, '×'. It is thus much easier to demonstrate the convergence of Δ' when re-orthogonalizations are used. Figure A2 shows how $\Delta'_{2/1}$ changes with increasing

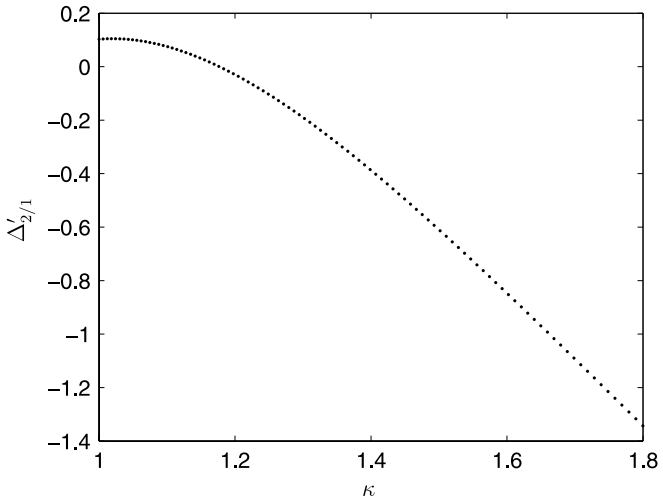

Figure A2. $\Delta'_{2/1}$ for the JET-like equilibrium described in the text as elongation, κ increases from 1 to 1.8. Each '·' represents a run of the T7 code.

elongation keeping all other factors of the equilibrium as described. Elongation has a stabilizing effect in this case.

References

[1] La Haye R J 2006 *Phys. Plasmas* **13** 055501
[2] Furth H P, Killeen J and Rosenbluth M N 1963 *Phys. Fluids* **6** 459
[3] Glasser A H, Greene J M and Johnson J L 1975 *Phys. Fluids* **18** 875
[4] Fitzpatrick R, Hastie R J, Martin T J and Roach C M 1993 *Nucl. Fusion* **33** 1533
[5] Connor J W *et al* 1988 *Phys. Fluids* **31** 577
[6] Cowley S C and Hastie R J 1988 *Phys. Fluids* **31** 426
[7] Chapman I T 2011 *Plasma Phys. Control. Fusion* **53** 013001
[8] Joffrin E *et al* 2005 *Nucl. Fusion* **45** 626
[9] Brennan D P *et al* 2002 *Phys. Plasmas* **9** 2998
[10] Brennan D P *et al* 2003 *Phys. Plasmas* **10** 1643
[11] La Haye R J *et al* 2008 *Nucl. Fusion* **48** 015005
[12] Pletzer A and Dewar R L 1991 *J. Plasma Phys.* **45** 427
[13] Pletzer A, Bondeson A and Dewar R L 1994 *J. Comput. Phys.* **115** 530
[14] Turco F and Luce T C 2010 *Nucl. Fusion* **50** 095010
[15] Gerhardt S P *et al* 2009 *Nucl. Fusion* **49** 032003
[16] Breslau J A *et al* 2011 *Nucl. Fusion* **51** 063027
[17] Gude A *et al* 1999 *Nucl. Fusion* **39** 127
[18] Fredrickson E D 2002 *Phys. Plasmas* **9** 548
[19] Kislov D A *et al* 2001 *Nucl. Fusion* **41** 1619
[20] Mercier C 1960 *Nucl. Fusion* **1** 47
[21] Grimm R C *et al* 1983 *Proc. 9th Int. Conf. on Plasma Physics and Controlled Nuclear Fusion Research 1982 (Baltimore, MD)* vol 3 (Vienna: IAEA) p 35
[22] Martin T J, Connor J W and Hastie R J 1991 *AEA Fusion Report* AEA FUS 91
[23] Glasser A H and Chance M S 1997 *Bull. Am. Phys. Soc* **42** 1848
[24] Atanasiu C V *et al* 2004 *Phys. Plasmas* **11** 5580
[25] Connor J W, Cowley S C, Hastie R J and Martin T J 1992 *Proc. 19th EPS Conf. on Controlled Fusion and Plasma Physics (Innsbruck, Austria)* ed W Freysinger *et al* (European Physical Society) vol 16C p 1393
[26] Chapman I T *et al* 2010 *Nucl. Fusion* **50** 045007
[27] Bussac M N *et al* 1977 *Proc. 6th Int. Conf. on Plasma Physics and Controlled Nuclear Fusion Research 1976 (Berchtesgaden, Germany)* vol 1 (Vienna: IAEA) p 269
[28] Bussac M N *et al* 1975 *Phys. Rev. Lett.* **35** 1638
[29] Manickam J 1987 *Nucl. Fusion* **27** 1461
[30] Holties H A *et al* 1996 *Nucl. Fusion* **36** 973
[31] Hastie R J and Hender T C 1988 *Nucl. Fusion* **28** 585
[32] Wahlberg C and Graves J P 2007 *Phys. Plasmas* **14** 110703
[33] Gimblett C G and Hastie R J 1998 *Proc. Joint Varenna-Lausanne Int. Workshop on the Theory of Fusion Plasmas, (Varenna, Italy, 31st August–4th September 1998)* (Bologna: Editrice Compositori) p 319
[34] Allfrey S J *et al* 1998 *Proc. 25th EPS Conf on Controlled Fusion and Plasma Physics (Prague, Czech Republic)* ed P Pavlov (European Physical Society) vol 22C p 2026
[35] Drake J F *et al* 1983 *Phys. Fluids* **26** 2509
[36] Cowley S C, Kulsrud R M, and Hahm T S 1986 *Phys. Fluids* **29** 3230
[37] Newcomb W A 1960 *Ann. Phys.* **10** 232
[38] Glasser A H 2010 *private communication*